Available online at www.sciencedirect.com

ScienceDirect

Procedia Structural Integrity 62 (2024) 710–723

Structural Integrity Procedia

www.elsevier.com/locate/procedia

II Fabre Conference – Existing bridges, viaducts and tunnels: research, innovation and applications (FABRE24)

Impact of hazard and fragility related uncertainties on seismic reliability assessment of existing structures

Lorenzo Hofer[a], Klajdi Toska[b], Mariano Angelo Zanini[a], Flora Faleschini[a], Carlo Pellegrino[a]

[a]*Department of Civil, Environmental and Architectural Engineering, University of Padova - Via Marzolo, 9 - 35131 Padova, Italy*
[b]*Laboratoire de Mécanique & Matériaux du Génie Civil-L2MGC, CY Cergy Paris Université - 5 Mail Gay Lussac, 95000 Neuville-sur-Oise, France*

Abstract

When dealing with seismic reliability assessment of structural systems, many uncertainty sources have to be handled by the risk analyst, who is asked to make some reasonable assumptions in order to carry out his/her seismic safety quantification. Indeed, slight changes in the definition of input parameters and/or the use of different empirical or analytical models can strongly impact the final reliability outcomes. The present work aims therefore to first analyse this issue clearly highlighting all possible sources of uncertainties that an analyst must face with, and then investigate their impact on the final reliability index variability via the use of a case-study represented by an existing multi-span steel-concrete composite bridge to better understand which of these sources is more impacting on the final estimates.

Keywords: seismic reliability; fragility analysis; PSHA; epistemic uncertainties; aleatory uncertainties; existing bridges.

1. Introduction

In the engineering practice, the seismic reliability assessment of an existing structure is commonly performed by coupling the seismic hazard curve with the seismic fragility curves. The former represents the seismicity of the site of interest and it is commonly computed via the so-called Probabilistic Seismic hazard Analysis (PSHA, Cornell 1968 and McGuire 1977), while the latter represent the probabilistic structural behavior of the considered structure and are commonly calibrated based on the outcomes of a set of numerical non-linear structural analyses. For both these two components involved the seismic structural assessment, several input parameters must be a priori fixed and different

2452-3216
10.1016/j.prostr.2024.09.098

models (e. g., empirical, numerical, etc.) have to be assumed. Thus results can be characterized by a significant uncertainty, especially for existing structures for which many parameters are unknown. Commonly, uncertainties are subdivided into two groups: epistemic uncertainties, related to the selection of the mathematical and formal models for describing the structural behavior and the seismic hazard, and aleatory uncertainty deriving from the intrinsic variability of natural phenomena, e.g. seismic events, and structural damaging (McGuire and Shedlock 1981). Currently, the so-called logic tree approach is one of the most adopted methods for handling all the different uncertainty sources in which each branch takes into account possible parameters' values and/or possible alternative models. Regarding the hazard analysis, the current seismic Italian hazard map (Stucchi et al. 2004) and the European Seismic Hazard Map (Giardini et al. 2014) are examples of application of the logic tree approach. More recently Zanini et al. 2019 developed a semi-analytical formulation for handling the uncertainty sources involved in the hazard computation. On the structural side, scientific literature widely discussed the role of uncertainty factors (Borgonovo et al. 2013, Pang et al. 2021 and Chen et al. 2023), highlighting how both aleatory and epistemic uncertainties can strongly impact the seismic fragility estimates (Dolsek 2008). However, even if several research has been done on how uncertainties impact singularly the seismic hazard and the fragility, few research tried to asses how the uncertainties related to hazard and fragility impact the final reliability assessment. Recently, the Authors did a first step in this direction, formalizing a general approach for handling all uncertainty sources linked to the definition of input parameters to be used in hazard and fragility calculations (Zanini et al. 2019), However, in the application only some uncertainty sources were explicitly considered. Hence, in this work the Authors want to fill this gap analyzing all the main aleatory and epistemic uncertainties that structural engineers and risk analysts must face with when performing a seismic reliability analysis. More details about the herein presented work can be found in Hofer et al. 2023.

2. Seismic reliability assessment mathematical formulation

Commonly in scientific literature, the mean failure rate λ_f is widely adopted for the seismic risk assessment of a structural system because it simply summarizes the site seismicity and the structural fragility and can be easily computed as:

$$\lambda_f = \int_{im} P[f|im] \cdot |d\lambda_{im}| \tag{1}$$

where λ_{im} represents the hazard curve of a specific site and $P[f|im]$ is the fragility curves representing the probabilistic structural behaviour of the analysed structure, i.e. the probability of reach and exceed a specific damage state for a given value of intensity measure im. In Eq. (1) $|d\lambda_{im}|$ represents the mean number of seismic events per year producing a shaking of exactly im, and can be computed from the hazard curve in the following way:

$$|d\lambda_{im}| = -\frac{d\lambda_{im}}{d(im)} d(im) \tag{2}$$

Then, the failure probability $P_{f,E,T}$ in a specific time window T can be computed from λ_f as

$$P_{f,E,T} = 1 - e^{-\lambda_f \cdot T} \tag{3}$$

and finally, the corresponding reliability index $\beta_{E,T}$ can be computed as the inverse of the standard normal cumulative density function evaluated in $P_{f,E,T}$

$$\beta_{E,T} = -\Phi^{-1}(P_{f,E,T}) \tag{4}$$

3. Uncertainty sources analysis

3.1. Seismic hazard

Nowadays, the PSHA is the most diffused approach for computing the hazard curve that associates to each level of ground motion intensity measure im the corresponding annual exceedance rate λ_{im} at the site of interest. The hazard curve can be computed in the following way

$$\lambda_{im} = \sum_{i=1}^{n_{ZS}} \upsilon_{m_{min,i}} \int_{m_{min,i}}^{m_{max,i}} \int_{r_{min,i}}^{m_{max,i}} P[IM > im|m,r] f_{M_i}(m)\, f_{R_i}(r) dm dr \tag{5}$$

where $f_{M_i}(m)$ represents the magnitude distribution of the i^{th} seismogenic zone (SZ) and $f_{R_i}(r)$ is the source-to-site distance distribution. hen $\upsilon_{m_{min,i}}$ is the rate of occurrence of earthquakes greater than a suitable minimum magnitude $m_{min,i}$ of the i^{th} SZ, while $P[IM > im|m,r]$ provides the exceedance probability of a given im value conditioned on a seismic event with a specific magnitude m and occurring at a distance r, and it is commonly computed via the so-called Ground Motion Prediction Equation (GMPE). In general, each quantity involved in Eq. (5) depends on several parameters that can be treated as random variables (RVs) thus making λ_{im} itself a RV. In this work all the RVs will be addressed with the Greek letter $\boldsymbol{\Theta}$. In $f_{M_i}(m, \boldsymbol{\Theta}_M)$ common parameters that can be treated as random are the maximum $M_{max,i}$ and minimum $M_{min,i}$ earthquake magnitude and the slope B_i of the Gutenberg–Richter (G-R) occurrence law. Furthermore, also $\upsilon_{m_{min,i}}$ can be considered as a RV ($\Upsilon_{m_{min,i}}$) related to the G-R law and thus included the parameters vector $\boldsymbol{\Theta}_M = \left[M_{max,i}, M_{min,i}, B_i, \Upsilon_{m_{min,i}}\right]$. Then also $f_{R_i}(r, \boldsymbol{\Theta}_R)$ can depends on some parameters (e.g., those describing the SZ geometry) that can be treated as RVs as well as the GMPE that relies on some regression parameters that can be assumed to be random ($\boldsymbol{\Theta}_{GMPE}$). Thus the final seismic hazard turns out to depend on a series of RVs $\boldsymbol{\Theta}_H = [\boldsymbol{\Theta}_M, \boldsymbol{\Theta}_R, \boldsymbol{\Theta}_{GMPE}]$ and Eq. (5) can be rewritten as

$$\lambda_{im}(\boldsymbol{\Theta}_H) = \sum_{i=1}^{n_{ZS}} \upsilon_{m_{min,i}} \int_{m_{min,i}}^{m_{max,i}} \int_{r_{min,i}}^{m_{max,i}} P[IM > im|m,r,\boldsymbol{\Theta}_{GMPE}] f_{M_i}(m, \boldsymbol{\Theta}_M)\, f_{R_i}(r, \boldsymbol{\Theta}_R) dm dr \tag{6}$$

Other than the aleatoric uncertainty strictly connected to the definition of the parameters' values, even the epistemic uncertainty, i.e. associated to the adopted GMPE or occurrence model, can be handled introducing a suitable probability mass function.

3.2. Structural fragility

The structural fragility analysis consists in the computation of $P[f|im]$ in Eq. (1) that represents the probability to reach and exceed a specific damage threshold, conditioned on a given value of intensity measure $IM = im$. In current engineering practice, fragility curves are computed vie the execution of a series of non-linear time history analysis (NLTHAs) in order to obtain a series of samples of the structural behaviour, commonly represented by a suitable engineering demand parameter (EDP, e.g. inter-storey drift ratio for framed buildings or top-displacement for cantilever structures) assumed to be a good metric for quantifying the structural damage. Then, in scientific literature, several procedures have been developed for computing the fragility curves starting from a sample of *n* couples of structural responses $[edp_1, edp_2 \ldots edp_n]$ and intensity measures $[im_1, im_2 \ldots im_n]$. Among all the most diffused are the so-called *Incremental Dynamic Analysis* (Vamvatsikos and Cornell 2004), the *Cloud Analysis* (Jalayer and Cornell 2003) and the *Multi-Stripes Analysis* (Baker 2015). In particular, this study adopts the *Cloud Analysis* procedure for deriving the fragility curves where fragilities are computed as

$$[f|im] = P\left[EDP > \overline{edp}|im\right] = 1 - P\left[EDP \leq \overline{edp}|im\right] = 1 - \Phi\left[\frac{ln(\overline{edp}) - ln(edp)}{\sigma}\right] \tag{7}$$

where $\overline{edp}$ represents the median value of the engineering demand parameter and $ln(edp)$ can be computed with a *ln*-linear regression model as:

$$ln(edp) = a_1 + a_2 \cdot ln(im) \tag{8}$$

with a_1 and a_2 coefficients of the linear regression. Finally, σ in Eq. (7) is the standard deviation of the demand conditioned on *im* that can be computed in the following way

$$\sigma = \sqrt{\frac{\sum_{i=i}^{n}\{ln(edp_i) - [a_1 + a_2 \cdot ln(im)]\}^2}{n-2}} \tag{9}$$

In this context, all the input data and modelling assumptions are the main uncertainty sources that structural engineers must face with: also in this case, aleatory and epistemic uncertainty sources can be identified. As regards aleatory uncertainties, when dealing with existing structures that can also often exhibit deterioration phenomena, material property values are the first unknown variables to be quantified. Then, also geometrical dimensions of structural elements can be considered as a source of uncertainty; however, most of cases relevant structures and bridges are often realized with a high-degree of compliance with design project and this issue implies the possibility to avoid the consideration of such source of uncertainty. Furthermore, since the set of accelerometric records used in the NLTHAs aims to represent the randomness of shaking scenario that can struck the analysed structure, the *n* ground motions intensities im_i represent themselves a set of realizations of the random variable IM. As a consequence, each data pair $[im_i; edp_i]$ is a random outcome of the structural response for a ground shaking level equal at im_i, and in turn also the regression parameters $\boldsymbol{\Theta}_F = [A_1, A_2, \Sigma]$ of the *ln*-linear regression model are RVs. Hence, the fragility curve formalized in Eq. (7) can be re-arranged as a function of $\boldsymbol{\Theta}_F$ as follows:

$$P[f|im; \boldsymbol{\Theta}_F] = P\left[EDP > \overline{edp}|im; \boldsymbol{\Theta}_F\right] \tag{10}$$

Other sources of epistemic uncertainty are also present when developing a numerical model; in particular referring to NLTHAs, the main modelling choices regard the adoption of a 2D or 3D model, the type of finite elements, the non-linearity modelling strategy, the constitutive models and the methodologies for the fragility assessment. For a wider description of all these aspects, the reader is referred to Hofer et al. 2023. Also in this case, the abovementioned uncertainty sources can be handled by introducing a probability mass function weighting each possible alternative.

3.3. Uncertainty indicators

According to the previous sections, Eq. (1) can be re-written for highlighting the dependance of $\lambda_f(\boldsymbol{\Theta})$ from a set of uncertain parameters treated as RVs and involved both in the hazard ($\boldsymbol{\Theta_H}$) and fragility ($\boldsymbol{\Theta_F}$) computation

$$\lambda_f(\boldsymbol{\Theta}) = \int_{im} P[f|im; \boldsymbol{\Theta_F}] \cdot |d\lambda_{im}; \boldsymbol{\Theta_H}| \tag{11}$$

As function of $\lambda_f(\boldsymbol{\Theta})$, the reliability index $\beta_{E,T}$ is itself function of $\boldsymbol{\Theta}$ and thus a RV. In the most general case, the expected value of the reliability index $E\left[\beta_{E,T}\right]$ can be computed by integrating $\beta_{E,T}(\boldsymbol{\Theta})$ over all the involved distributions $f(\boldsymbol{\Theta})$, more formally as:

$$E\left[\beta_{E,T}\right] = \int_{\boldsymbol{\Theta}} \beta_{E,T}(\boldsymbol{\Theta}) f(\boldsymbol{\Theta}) d\boldsymbol{\Theta} \tag{12}$$

he analytical solution of Eq. (12) commonly involves nasty calculations, and thus numerical sampling methods, as the Monte Carlo Simulation (MCS), are needed. Thank to these methods, it is possible to sample random vectors from

the parameter distributions and along the logic tree branches, for withdrawing a series of $\beta_{E,T,i}$ samples from which interpolate a suitable probability density function *pdf* of the reliability index $f_{B_{E,T}}(\beta_{E,T})$. This pdf encloses all the information about the seismic reliability of the investigated structure since it provides the central tendency and the dispersion introduced from all the different considered uncertainty sources. Thus, it is possible to compute:

1. The *Expected Seismic Reliability Index* as

$$E\mu_{B_{E,T}} = E[B_{E,T}] = \int \beta_{E,T} \cdot f_{B_{E,T}}(\beta_{E,T}) d\beta_{E,T} \tag{13}$$

2. The *Seismic Reliability Index Dispersion* as

$$\delta_{B_{E,T}} = \frac{\sigma_{B_{E,T}}}{\mu_{B_{E,T}}} = \frac{\sqrt{\int (\beta_{E,T} - \mu_{B_{E,T}})^2 \cdot f_{B_{E,T}}(\beta_{E,T}) d\beta_{E,T}}}{\int \beta_{E,T} \cdot f_{B_{E,T}}(\beta_{E,T}) d\beta_{E,T}} \tag{14}$$

4. Case Study

The general framework has been applied to an existing multi-span steel-concrete composite bridge located in the Treviso district (lat. 45.60, long. 12.32), north-eastern Italy. Four 30 m spans and 5.5 m height piers characterize the bridge. The bridge girder is composed by two longitudinal continuous steel beams and by a series of transversal steel beams, collaborating with a reinforced concrete (RC) slab. Fig. 1 shows the main geometric characteristic of the bridge.

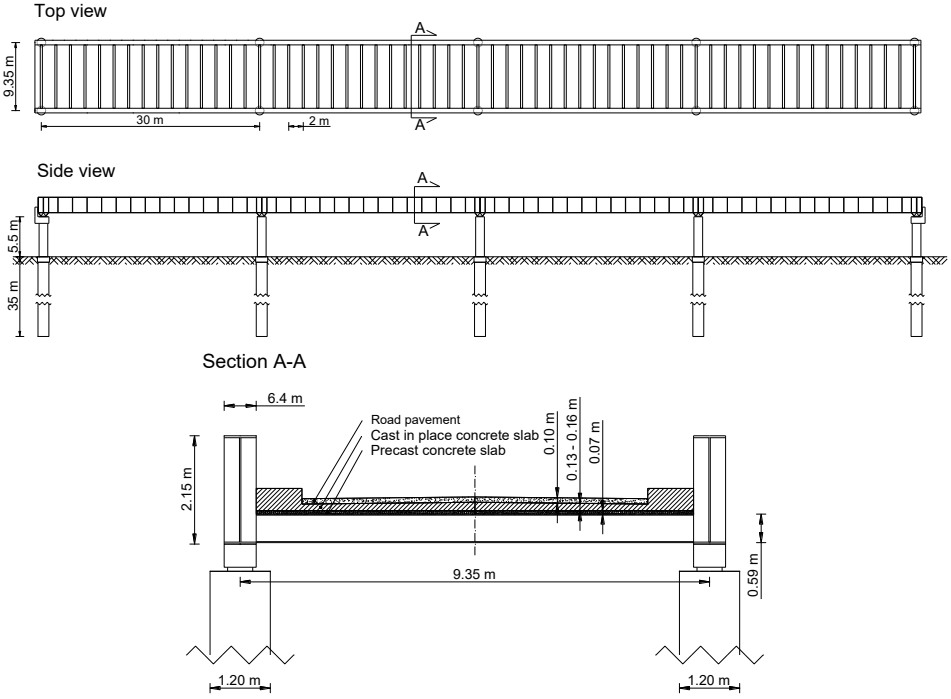

Fig. 1. Main geometrical characteristics of the bridge (Hofer et al. 2023).

4.1. Uncertainty sources in the seismic hazard

For the seismic hazard definition, a PSHA has been carried out considering all the possible relevant uncertainty sources. In detail, the seismogenic source zone model ZS9 detailed in Meletti et al. ZZZ has been adopted, using Gutenberg-Richter (G-R) recurrence laws for each of the 12 SZs contributing to the seismic hazard (Fig. 2a). While the seismogenic source model geometry has been assumed deterministic, the main parameters characterizing the G-R relationship (i.e., $m_{max,i}$, b_i and $\nu_{m_{min,i}}$) of each source have been considered random. Fig. 2b shows for each i^{th} SZ the mean value of each parameter (retrieved from Barani et al. 2009), the lower (subscript "1") and the upper (subscript "3") value. The mean value was weighted 0.5, while the other two alternatives 0.25.

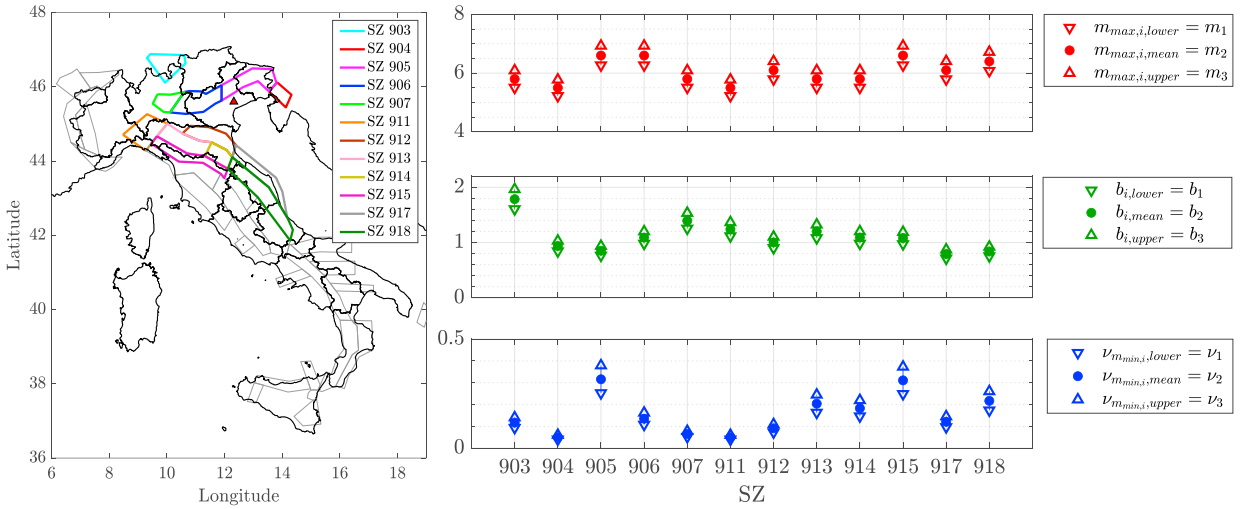

Fig. 2. (a) Bridge site and adopted seismogenetic source model and (b) adopted G-R parameters values (adapted from Hofer et al. 2023).

In this study, two different GMPEs are adopted for taking into account the epistemic uncertainty coming from this element of the seismic hazard: firstly, the one of Ambraseys et al. 1996 (hereafter *ABS*) weighted of 0.6 for its similarity with the official Italian seismic hazard map, secondly the one of Bindi et al. 2011 (hereafter *BIN*) computed from data of the Italian strong motion database ITACA (Pacor et al. 2011). Fig. 3 shows all the computed hazard curves and the entire logic tree adopted for describing the main uncertainty sources involved in the hazard computation, $\boldsymbol{\Theta}_H = \left[M_{max,i}, M_{min,i}, \Upsilon_{m_{min,i}}, GMPE\right]$.

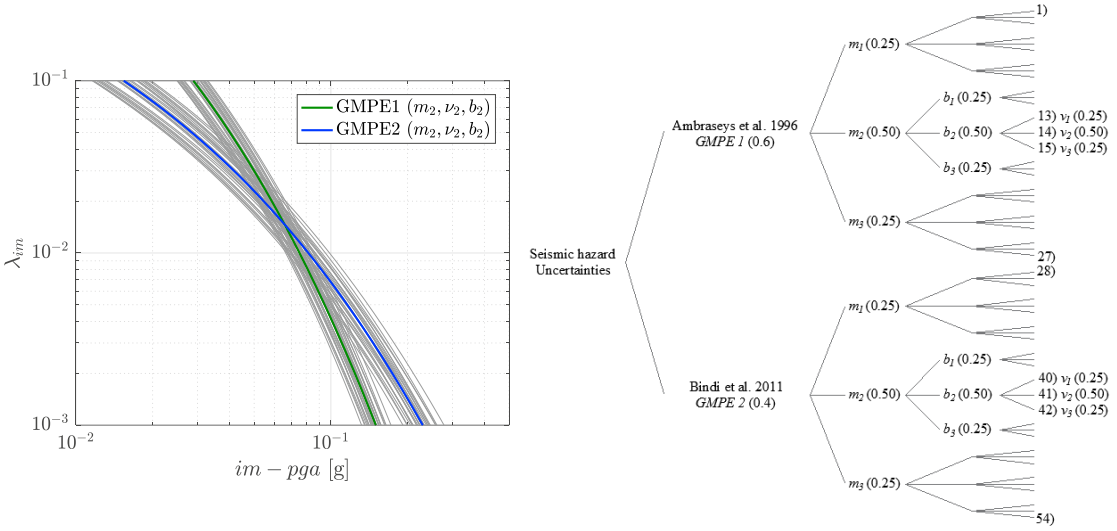

Fig. 3. Computed hazard curves and logic tree for the seismic hazard (adapted from Hofer et al. 2023).

4.2. Uncertainty sources in the seismic fragility

Regarding the uncertainties related to the development of the fragility curves, four main uncertainty sources are herein considered: the soil stratigraphy parameters, the steel material properties, the columns non-linear modelling and the number of accelerograms to be used for deriving the fragility curves. The bridge is made by a steel-concrete composite deck, whose main and secondary beams are made of Fe510C and Fe360B steels, respectively. The RC slab has a varying thickness (i.e. 0.23 m in the middle of the roadway section, decreasing to 0.20 m in the borders) and it is made of concrete with a characteristic cubic compressive strength (R_{ck}) of 35 MPa. The bridge steels beams grillage is modelled with 1D beam element, whereas 2D plate elements are used for the concrete slab. Fig. 4 shows the adopted finite element model and some details of it. Details about the geometry and the materials' properties of the bridge's pier and foundations are reported in Hofer et al. 2023.

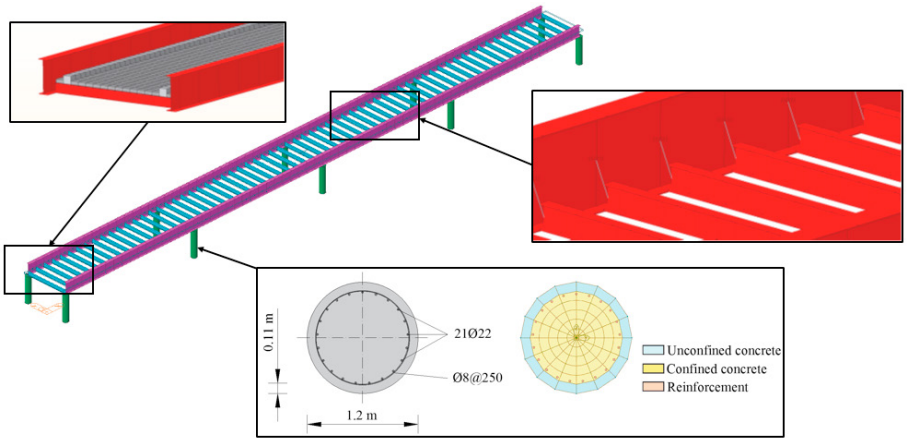

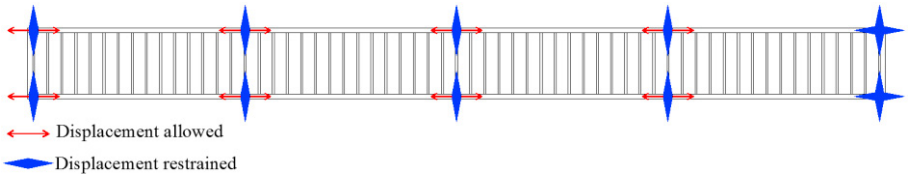

Fig. 4. FE model of the bridge case study (Hofer et al. 2023).

Foundations have been modelled by adopting general element links able to represent the non-linear translational and rotational behavior of the foundation piles. In detail, a series of pushover analyses have been performed to calibrate the overall non-linear behavior of the foundational system. Fig. 5 shows the soil stratigraphy with the friction angle ϕ_{mean} characterizing the sand layers, and the cohesion ($C_{u,mean}$) proper of the clay layers; for each layers also upper and lower values have been considered.

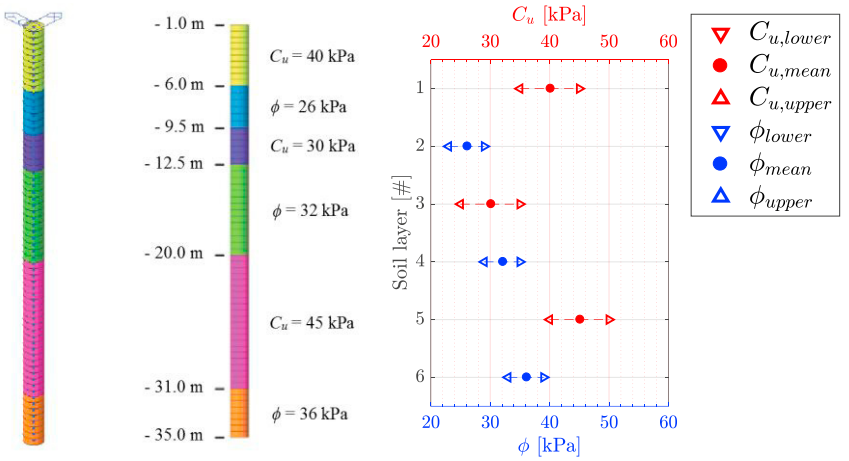

Fig. 5. Soils stratigraphy and soil property values (Hofer et al. 2023).

Finally, Fig. 6 shows the final curves adopted for the characterization of the overall translational (a) and rotational (b) behaviours of the general link used as a lumped model for the foundations, namely F_1 (ϕ_{mean} and $C_{u,lower}$), F_2 (ϕ_{mean} and $C_{u,mean}$), and F_3 (ϕ_{mean} and $C_{u,upper}$). A *pmf* is adopted for representing this uncertainty source, with weights assumed equal to 0.25 for F_1 and F_3 cases, and 0.5 for F_2 one. For further information on the computation of the curves in Fig. 6, the reader s referred to Hofer et al. 2023.

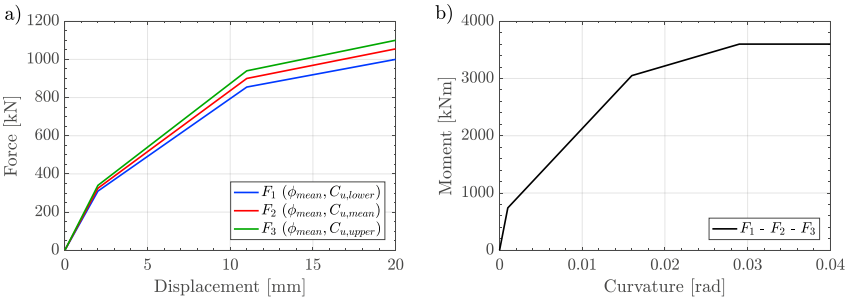

Fig. 6. Translational (a) and rotational (b) behavior of the general link adopted for representing the foundations response (Hofer et al. 2023).

Then, regarding the materials properties, the reinforcement steel was assumed to be random. Based on the distribution of the test results for FeB44k steel type (Verderame et al. 2011), strength values of 494, 526 and 558 MPa, respectively addressed as S_1, S_2 and S_3 and weighted 0.25, 0.50 and 0.25 were adopted in the analysis. As regard the numerical modelling of the non-linearity, in this work both the concentrated plasticity (i.e. plastic hinges, *PH*) and fibres sections (*FIB*) have been considered as two viable alternatives, using respectively the *Multi-Linear Plastic Pivot Type hysteresis Model* of Dowell et al. 1998 for the former case, and the Menegotto and Pinto 1973 and the Mander et al. 1988 models for the latter one. As regards the weighting procedure, weights of 0.4 and 0.6 has been assumed for *PH* and *FIB* modelling strategies, being the latter more reliable according to current scientific literature. For deriving fragility curves, 55 simulations for each of the 18 logic tree branches were performed, for a total number of 990 NLTHAs. Fragility curves have been then extracted via the use of the *Cloud Analysis* method with reference to four damage states ds_i (i.e., ds_1 = *slight*, ds_2 = *moderate*, ds_3 = *extensive* and ds_4 = *complete*), using the pier's top displacement Δ as EDP. Further details on the adopted accelerometric records and on the derivation of the fragility curves can be found in Hofer et al. 2023. Finally, since uncertainty related to record-to-record variability can strongly impact fragility estimates (Zanini et al. 2017), a bootstrap resampling strategy has been used for considering also this uncertainty source. In particular, a re-sampling of 40 over 55 records has been performed subsequently deriving for each sampled cloud of 40 data pairs $[pga_i; \Delta_i]$, the corresponding fragility curve. Fig. 7a, Fig 7b and Fig. 7c show respectively the convergence of a_1, a_2 and σ, while Fig. 7d shows all regression lines computed from the samples of 40 over 55 data pairs, for the *FIB*-F_2-S_2 configuration. The bundle of fragility curves for each damage state has been summarized in three main curves, an upper (A_1), a median (A_2) and a lower (A_3) ones, representative of the quartiles and median envelopes of sampled fragilities. Fig. 8 shows for sake of example A_1, A_2, and A_3 fragility envelopes for each damage state for the *FIB*-F_2-S_2 configuration. Finally, Fig. 9 shows the entire logic tree adopted for describing the main uncertainty sources involved in the fragility computation, $\boldsymbol{\Theta}_F = [NL, F, S, A]$.

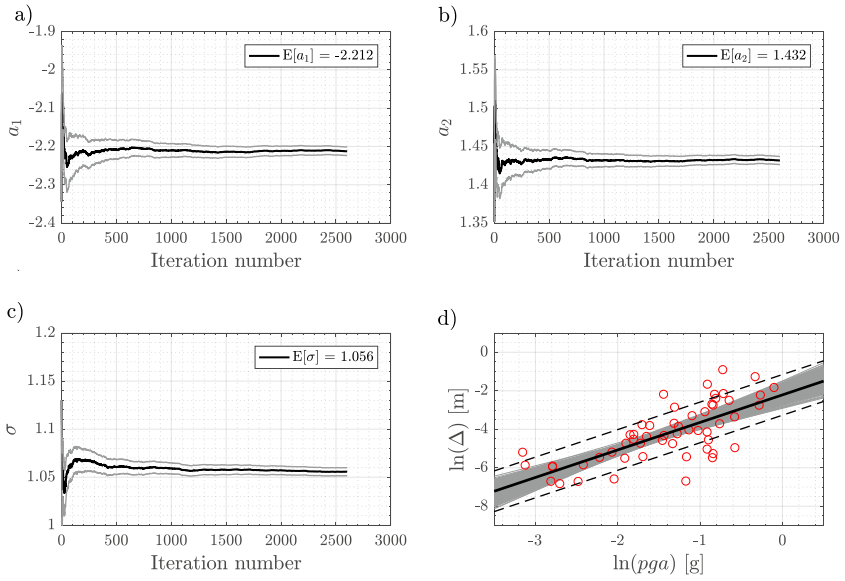

Fig. 7. Example of fragility curve resampling for the case of fiber model (*FIB*), with foundations F_2 and steel S_2: convergence of a_1 (a), a_2 (b) and σ (c), and bootstrap resampling (d) (Hofer et al. 2023).

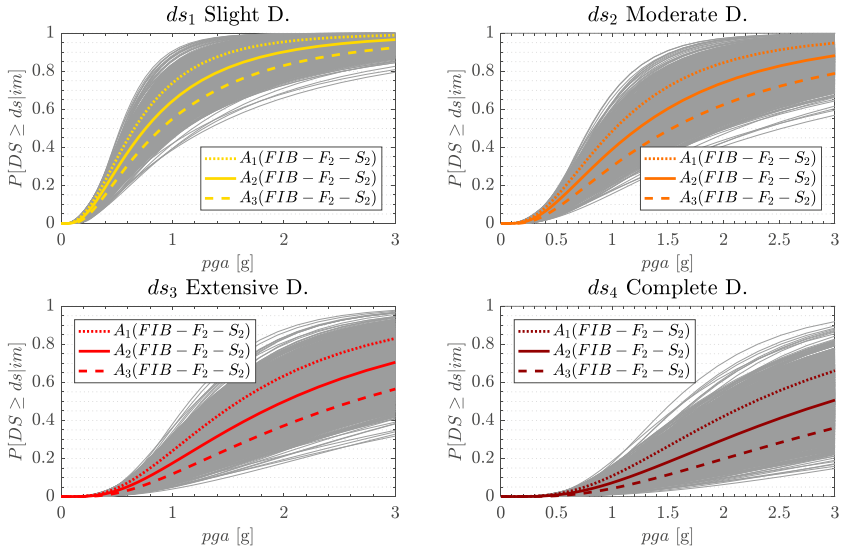

Fig. 8. Upper (A_1), median (A_2) and lower (A_3) fragility envelopes for each damage state *FIB*-F_2-S_2 configuration (Hofer et al. 2023).

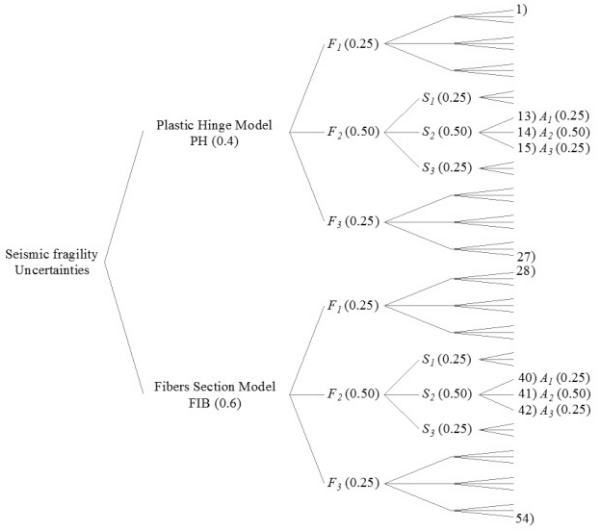

Fig. 9. Logic tree for the structural fragility (Hofer et al. 2023).

5. Results

One-year reliability index β has been first computed according to Eq. (4) for the four main branches, i.e. those derived from the combination of the two different GMPEs and the two non-linearity modelling techniques; and assuming the mean value for the remaining parameters (m_2, ν_2, b_2 and F_2, S_2 and A_2). Results are listed in Table 1 and shows that for each damage state, the model with the concentrated plastic hinges, combined with the hazard derived from the GMPE of Ambraseys et al. 1996, leads to the lowest seismic reliability (i.e. β values equal to 3.32, 3.64, 3.96 and 4.22 respectively for ds_1, ds_2, ds_3 and ds_4). On the contrary, the highest reliability values are obtained from the combination of fibres section models with the Bindi et al. 2011 GMPE.

Table 1. Reliability index values for the four main logic tree branches.

	ds_1	ds_2	ds_3	ds_4
ABS-PH	4.66	4.33	3.94	3.53
ABS-FIB	4.99	4.64	4.23	3.81
BIN-PH	4.22	3.96	3.64	3.32
BIN-FIB	4.46	4.18	3.84	3.51

Considering all the uncertainty sources coming from both the hazard and the fragility modules, a logic tree of 2916 branches was obtained. Fig. 10 shows the matrix of weights w of all the investigated logic tree branches (highest weight of 0.0056 for *ABS*, m_2, v_2, b_2, F_2, S_2 and A_2).

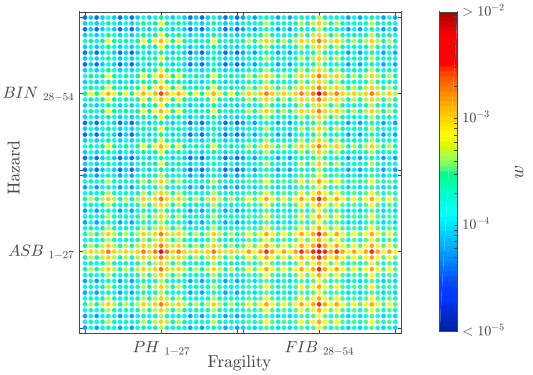

Fig. 10. Weights of all the logic tree branches (Hofer et al. 2023).

Fig. 11 shows all the 2916 computed values of the reliability index while Fig. 12 shows the reliability index distributions obtained by coupling the reliability index values with the associated branches weights. The effect of the two main branches (i.e. the GMPE and the non-linearity modelling strategy) is clearly identifiable, since dots tend to produce four graduals steps on the 3D representation of the reliability index β matrix. The expected yearly reliability index $\mu_{B_{E,T=1}}$ and the reliability index dispersion $\delta_{B_{E,T=1}}$, computed according to Eqs. (13, 14), are also shown in Fig. 12.

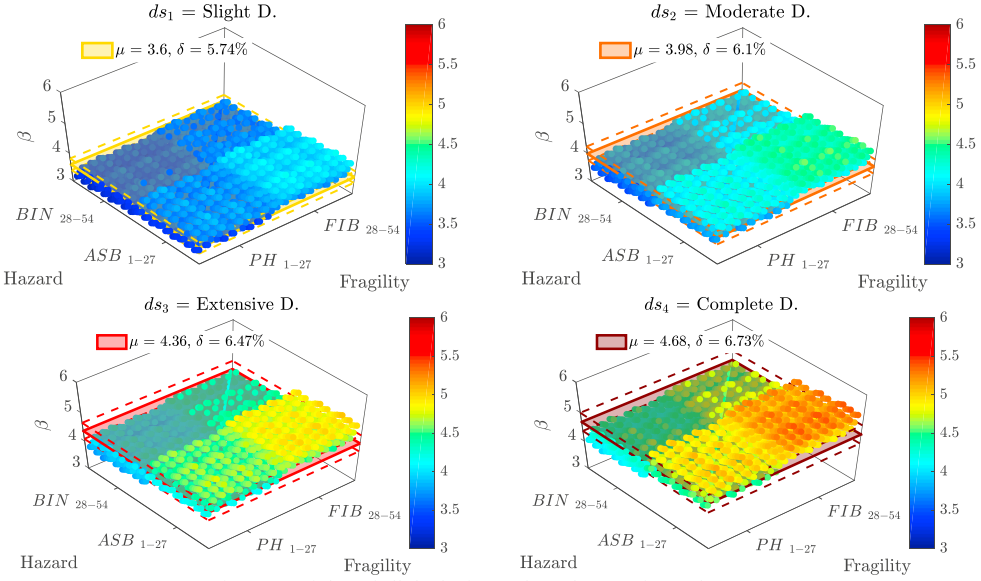

Fig. 11. Weights of all the logic tree branches (Hofer et al. 2023).

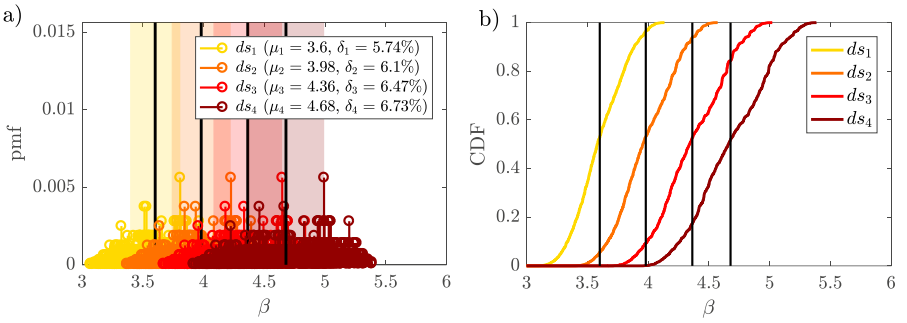

Figure 12. Reliability index *pmf* (a) and Reliability index CDF (b) for every damage state (Hofer et al. 2023).

An in-depth uncertainty quantification analysis has been also carried out with the aim to identify which parameters mostly contribute to the reliability index uncertainty. To this aim, numerical simulations have been rerun by imposing each time a different parameter as deterministic (i.e. removing its uncertainty source).

Fig. 13a shows the % variation of the yearly reliability index dispersion $\delta_{B_{E,T=1}}$, with the assumption in turn of one deterministic parameter. The GMPE seems to be the parameter most contributing to $\delta_{B_{E,T=1}}$, whereas when the GMPE is assumed deterministic, a significant reduction of yearly reliability index dispersion $\delta_{B_{E,T=1}}$ can be obtained. The reduction is not constant for the four damage states, by it is higher for the Complete Damage state (about -33 %), and lower for the Slight Damage State (-14 %). The second parameter that mostly affects $\delta_{B_{E,T=1}}$ is represented by non-linearity modelling strategy: in detail, when the uncertainty arising from it is not accounted for, the $\delta_{B_{E,T=1}}$ decreases of about 10 %. In this case, the higher reduction has been obtained for the ds_1 (-15 %), while the lower reduction for ds_4 (-8.7 %). The third parameter that most influences the yearly reliability index dispersion $\delta_{B_{E,T=1}}$ is the number of the accelerograms adopted for the execution of NLTHAs (reduction of -9 %, with little variation within the four damage states). The uncertainties related to the remaining investigated parameters (i.e. m_i, b_i, ν_i, F_i and S_i) seem to have a negligible impact on $\delta_{B_{E,T=1}}$. As regards the impact of the one-year expected reliability index $\mu_{B_{E,T}}$, the adoption of a deterministic parameter leads to variations in the order of 4 %, as shown in Fig. 13b.

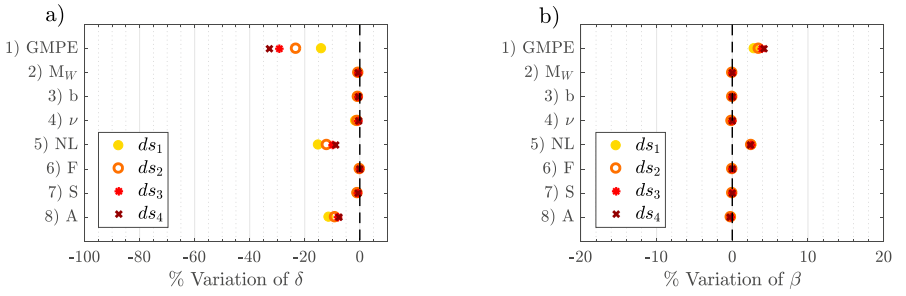

Figure 13. Reduction of $\delta_{B_{E,T=1}}$ (a) and variation of $\mu_{B_{E,T}}$ (b) adopting one deterministic parameter.

Hence, the uncertainty quantification has been carried out considering also in turn a couple of deterministic parameters. Results showed that assuming the GMPE and the non-linearity modelling strategy as deterministic provides the higher $\delta_{B_{E,T=1}}$ reduction, about -56 % for ds_4 and – 44 % for ds_1. When the number of records (A) and the GMPE are assumed as deterministic, a reduction of – 47 % is obtained for ds_4, while a reduction of – 31 % is obtained for ds_1. Further considerations and a sensitivity analysis on the logic-tree branches weights are available in Hofer et al. 2023.

6. Conclusions

This study aims at investigating the effects of the main uncertainty sources that are usually involved in the seismic reliability assessment of a structure. To this aim, a general formulation able to formally treats all the uncertainty sources is proposed and then applied to a case study. This work shows that several uncertainty sources are involved in both the seismic hazard and in the structural fragility. In the analysed case study, eight uncertainty were considered and then combined by adopting a logic tree approach with 2916 total branches. The highest reliability index dispersion of 6.73% was obtained for the Complete Damage State, while the lowest one was obtained for the Slight Damage State (5.74%). Then a detailed sensitivity analysis was carried out for ranking the uncertainty sources in relation to their impact on the overall reliability index dispersion. Results showed that the uncertainty associated to the GMPE selection is the most relevant, followed by the adopted non-linearity modelling technique and the number of accelerometric records adopted for the structural analysis. Together, the choice of the GMPE, the non-linearity modelling technique and the number of accelerometric records represents almost the 80% of the overall reliability index dispersion. Furthermore, results showed that uncertainty involved in the seismic hazard computation are comparable to those involved in the structural fragility assessment. For these reasons, neglecting one if these two implies a significant underestimation of the reliability index dispersion.

References

Ambraseys, N. N., Simpson, K. A., Bommer J.J. 1996. Prediction of horizontal response spectra in Europe, Earthquake Engineering & Structural Dynamics, 25: 371–400.

Baker, J.W. 2015 Efficient analytical fragility function fitting using dynamic structural analysis Earthq Spectra, 31(1): 579-599.

Barani, S., Spallarossa, D., Bazzurro, P. 2009 Disaggregation of probabilistic ground motion hazard in Italy. Bull Seismol Soc Am, 99(5):2638–61.

Bindi, D., Pacor, F., Luzi, L., Puglia, R., Massa, M., Ameri, G., Paolucci, R. 2011. Ground motion prediction equations derived from the Italian strong motion database. Bull Earthq Eng, 9:1899–920.

Borgonovo, E., Zentner, I., Pellegri, A., Tarantola, S., de Rocquigny, E. 2013. On the importance of uncertain factors in seismic fragility assessment. Reliab Eng Syst Saf 109: 66–76.

Chen, K., Pang, R., Xu, B. 2023. Stochastic dynamic response and seismic fragility analysis for high concrete face rockfill dams considering earthquake and parameter uncertainties. Soil Dyn Earthq Eng, 167:107817.

Cornell, C., 1968. Engineering seismic risk analysis. Bull Seismol Soc Am 58(5), 1583-606.

Dolsek, M. 2008 Incremental dynamic analysis with consideration of modelling uncertainties. Earthq Eng Struct Dy, 38(6):805–25.

Giardini, D., Woessner, J., Danciu, L. 2014. Mapping Europe's Seismic Hazard. Eos, 95(29):261–2.

Hofer, L., Toska, K., Zanini M.A. 2023. Impact of epistemic and aleatory uncertainties on the seismic reliability assessment of existing structures. Structures 57:105235.

Jalayer, F., Cornell, C.A. 2003. Direct probabilistic seismic analysis: implementing non-linear dynamic assessments. Stanford University.

Mander, J.B., Priestley, M.J.N., Park, R. 1988 Theoretical stress-strain model for confined concrete. J Struct Eng, 114(8):1804–26.

McGuire, R.K., 1977. Effects of uncertainties in seismicity on estimates of seismic hazard for the east coast of the United States. Bull Seismol Soc Am 67, 827-48.

McGuire, R.K., Shedlock, K.M. 1981. Statistical uncertainties in seismic hazard evaluations in the United States. Bull Seismol Soc Am 71, 1287–308.

Meletti, C., Galadini, F., Valensise, G., Stucchi, M., Basili, R., Barba, S., et al. 2008. A seismic source zone model for the seismic hazard assessment of the Italian territory. Tectonophysics, 450(1-4):85–108.

Menegotto, M., Pinto, P.E. 1973. Method of analysis for cyclically loaded reinforced concrete plane frames including changes in geometry and non-elastic behavior of elements under combined normal force and bending. In: Proceedings IABSE symposium of resistance and ultimate deformability of structures acted on by well defined repeated loads, vol. 13. Lisbon, Portugal: International Association of Bridge and Structural Engineering. p. 15–22.

Pacor, F., Paolucci, R., Ameri, G., Massa, M., Puglia, R. 2011. Italian strong motion records in ITACA: overview and record processing, Bulletin of Earthquake Engineering, 9: 1741-1759.

Pang, R., Xu, B., Zhou, Y., Song, L. 2021. Seismic time-history response and system reliability analysis of slopes considering uncertainty of multi-parameters and earthquake excitations. Comput Geotec, 136:104245.

Stucchi, M., Meletti, C., Montaldo, V., Akinci, A., Faccioli, E., Gasperini, P., et al. 2004. Pericolosità sismica di riferimento per il territorio nazionale MPS04. Istituto Nazionale di Geofisica e Vulcanologia (INGV).

Vamvatsikos. D., Cornell, CA. 2004. Applied incremental dynamic analysis, Earthquake Spectra, 20(2):523–53.

Verderame, G.M., Ricci, P., Esposito, M., Sansiviero, F.C. 2011. Le caratteristiche meccaniche degli acciai impiegati nelle strutture in c.a. realizzate dal 1950 al 1980. Atti del XXVI Convegno Nazionale AICAP "Le prospettive di sviluppo delle opere in calcestruzzo strutturale nel terzo millennio", Padova, 19-21 Maggio

Zanini, M.A., Hofer, L., Faleschini, F., Pellegrino, C. 2017 The influence of record selection in assessing uncertainty of failure rates. Ingegneria Sismica, 34:30–41.

Zanini, M.A., Hofer, L., Toska, K. 2019. A semi-analytical formulation for accounting uncertainties of hazard parameters in structural seismic reliability analysis. Eng Struct, 192:18–29.

Zanini, M.A., Hofer, L. 2019. Center and Characteristic Seismic Reliability as new indexes for accounting uncertainties in seismic reliability analysis. Soil Dyn Earthq Eng, 123:110–23.